

Sulfur-containing amino acids in 7TMRs: molecular gears for pharmacology and function

Arnau Cordomí¹, José C. Gómez-Tamayo¹, Véronique Gigoux², and Daniel Fourmy²

¹Laboratori de Medicina Computacional, Unitat de Bioestadística, Facultat de Medicina, Universitat Autònoma de Barcelona, 08193 Bellaterra, Barcelona, Spain

²Université de Toulouse 3, EA, 4552, Toulouse, France

Seven-transmembrane receptors (7TMRs) mediate the majority of physiological responses to hormones and neurotransmitters in higher organisms. Tertiary structure stability and activation of these versatile membrane proteins require formation or disruption of complex networks of well-recognized interactions (such as H-bonds, ionic, or aromatic–aromatic) but also of other type of interactions which have been less studied. In this review, we compile evidence from crystal structure, biophysical, and site-directed mutagenesis data that indicate or support the importance of interactions involving Met and Cys in 7TMRs in terms of pharmacology and function. We show examples of Met/Cys–aromatic and Met–Met interactions participating in ligand binding, in tuning the orientation of functionally important aromatic residues during activation or even in modulating the type of signaling response. Collectively, data presented enlarge the repertoire of interactions governing 7TMR functioning.

General considerations about structural features of 7TMRs

7TMRs, also known as G-protein-coupled receptors (GPCRs), mediate nearly all human cellular responses to hormones and neurotransmitters. Therefore, they are one of the most attractive target families for drug discovery and already comprise approximately 30% of current therapeutic agents on the market [1]. Significant advances in crystallization of 7TMRs have permitted elucidation of the structures of many receptors [2–22]. These represent invaluable tools for understanding how 7TMRs function at residue and molecular levels. There is considerable evidence that, despite a remarkable diversity in ligands, the ligand-encoded extracellular signal is propagated from the binding site into intracellular domains through a common activation mechanism. These would subsequently trigger further signaling pathways. For example, when 7TMRs activate G proteins, an outward tilt of the intracellular part of transmembrane (TM) 6 occurs together with a

movement of TM5 towards TM6 and a side chain extension of Arg^{3.50} within the (E/D)RY motif in TM3 towards the protein core, to interact with the highly conserved Tyr^{5.58} in TM5 and with Tyr^{7.53} of the NPxxY motif in TM7 (superscripts refers to the Ballesteros and Weinstein numbering scheme [23]) [24–28]. All these steps require formation and breakage of noncovalent interactions such as ionic, hydrogen bond, and dispersion-stabilized interactions (including aliphatic–aliphatic, aromatic–aromatic, aromatic–aliphatic), most of which are well described (see [Glossary](#) and [Table 1](#)). There are, however, other types of dispersive interactions present in 7TMRs that are yet not well characterized and less recognized. This is the case of interactions involving sulfur-containing amino acids (Cys and Met) and in particular between Met/Cys and aromatic and between two Met or Cys residues. The nature of such interactions is primarily dispersive, although it is generally considered to involve a significant electrostatic component as well [29]. In fact, the range of geometries observed for these interactions in crystal structures reveals the existence of contributions with different physicochemical origin: S⋯π (in Met–aromatic and Cys–aromatic), C–H⋯π interactions (in Met–aromatic), C–H⋯S hydrogen bonds (in Met–Met, Cys–aromatic, and Met–aromatic), S–H⋯S hydrogen bonds (in Cys–Cys) and S–H⋯π (in Cys–aromatic) [30–36]. It is important to outline that the large polarizability of sulfur also enhances the interactions involving –CH₂– and –CH₃ groups attached to sulfur compared to aliphatic chains (as, e.g., in Ile or Leu).

In the late 1970s, Morgan and coworkers observed a high frequency of contacts between sulfur-containing residues and aromatic residues in proteins, and even found

Glossary

Dispersion: interaction between nonpolar molecules due to electron redistribution caused by proximity between molecules. It represents the main part of the total interaction force in condensed matter.

Intermolecular forces: attraction and/or repulsion between neighboring particles.

van der Waals forces: weak interactions between molecules other than Coulomb interactions. They include dipole-induced dipole and induced dipole-induced dipole (dispersion) interactions.

Corresponding author: Fourmy, D. (Daniel.Fourmy@inserm.fr).

Keywords: GPCR; crystal structure; site-directed mutagenesis; molecular modeling.

0165-6147/\$ – see front matter

© 2013 Published by Elsevier Ltd. <http://dx.doi.org/10.1016/j.tips.2013.03.008>

Table 1. Summary of intermolecular forces in proteins

	Type of interaction	Factors responsible for interaction	Energy range (kcal/mol)	Distance dependency on energy	Example
Coulomb	Ion-ion	Ion charge	20–40	1/r	$-\text{NH}_3^+ \cdots \text{OOC}-$
	Ion-dipole (H-bond)	Ion charge, dipole magnitude	10–25	1/r ²	$-\text{NH}_3^+ \cdots \text{O}=\text{C}<$
	Dipole-dipole (H-bond)	Dipole magnitude, electronegativity	2–7	1/r ³	$>\text{C}=\text{O} \cdots \text{HN}<$
van der Waals	Dipole-induced dipole	Dipole magnitude, polarizability	0.5–2.5	1/r ⁴	$-\text{OH} \cdots -\text{CH}_3$
	Dispersion	Polarizability	0.1–3	1/r ⁶	$-\text{CH}_3 \cdots -\text{CH}_3$

large stacked arrangements composed of aromatic and Met or Cys residues [37]. Further studies also demonstrated that Cys/Met–aromatic interactions were fairly common in protein crystal structures and that Met was as likely as Phe or Trp to be near another Trp, with the majority of interactions facing the ring [30–32]. Recently, several attempts to determine binding energies for model systems representing sulfur–aromatic interactions have been performed [33,34,38]. From experimental studies of modeled peptides in water, sulfur–aromatic interactions were estimated to contribute up to ~ 2 kcal/mol [39]. However, these interactions are probably even stronger when they occur in nonpolar environments, as for example, the protein interior. Recent high level *ab initio* calculations gave interaction energies up to ~ 3 –3.5 kcal/mol for side chain analogs of Met–Phe, Cys–Phe, Cys–Cys, and Met–Met interactions (J.C. Gómez-Tamayo *et al.*, in preparation). This puts these interactions at a similar level (and even higher) in terms of strength to other commonly accepted interaction types such as aromatic–aromatic (the energy of interaction between two Phe residues is 2.4 kcal/mol [40–42]).

Interactions involving sulfur-containing amino acids in 7TMR crystal structures

Analysis of 17 7TMR crystal structures corresponding to distinct members of the family available revealed the existence of 216 Met–aromatic, 210 Cys–aromatic, 22 Met–Met, 22 Cys–Met, and 3 Cys–Cys (excluding disulfide) interactions (Tables 2 and 3). This means that, on average,

each receptor contains 25 sulfur–aromatic and 3 sulfur–sulfur interactions. The low prevalence of Cys–Cys interactions is due to involvement of Cys in disulfide bridges or hydrogen bond interactions and also to its shorter side chain (and thus smaller surface accessibility) compared to Met. Remarkably, it turns out that 47% of aromatic residues present in 7TMRs are involved in interactions with Met and Cys residues, mostly Met–Phe, Met–Tyr, and Cys–Phe pairs. Furthermore, Met/Cys–aromatic and Met/Cys–Met/Cys interactions in 7TMRs are often alternated with aromatic–aromatic interactions, forming large stacked arrangements such as those described by Morgan *et al.* [37]. Although their functional significance is not fully understood in 7TMRs, it is likely that these may constitute molecular machineries stabilizing specific receptor conformations or transmitting structural changes from the extracellular to the cytoplasmic interface, promoting or inhibiting binding to G proteins and/or other signaling proteins.

One of the most remarkable examples of such a stacked arrangement can be found in the β_2 adrenergic receptor (β_2 AR). Specifically, a network of interactions extends from Cys116^{3,35} to Trp32^{1,31} and involves consecutive Met–aromatic, Met/Cys–Met, and aromatic–aromatic interactions besides the ligand-binding site (Figure 1A). In the core of this network, Tyr316^{7,43} participates in a Met–aromatic interaction with Met82^{2,53} (see below) and also forms a hydrogen bond with Asp113^{3,32}, the most critical residue for ligand binding in amine receptors. This suggests that

Table 2. Summary of interactions involving sulfur-containing amino acids in the crystal structures of 7TMRs

Receptor	Organism	PDB id Refs	Met–Aro	Met–Met	Cys–Aro	Cys–Cys	Cys–Met	Total ^a
Rhodopsin	Bovine	1GZM [2]	25	2	17	0	1	45
Rhodopsin	Squid	2Z73 [4]	22	7	12	1	2	44
β_2 -Adrenergic	Human	2RH1 [5]	9	3	11	0	2	25
β_1 -Adrenergic	Turkey	2VT4 [7]	9	2	7	0	2	20
H1 Histamine	Human	3RZE [8]	13	1	11	0	3	28
D3 Dopamine	Human	3PBL [9]	9	1	11	0	0	21
M2 Muscarinic	Human	3UON [10]	9	3	12	1	1	26
M3 Muscarinic	Rat	4DAJ [11]	8	0	10	1	0	19
κ OR Opioid	Human	4DJH [12]	18	0	14	0	2	34
μ OR Opioid	Mouse	4DKL [13]	18	0	15	0	2	35
δ OR Opioid	Mouse	4EA3 [14]	12	0	12	0	3	27
NO/FQ Opioid	Human	4EJ4 [15]	14	0	10	0	1	25
A _{2A} Adenosine	Human	4EYI [16]	12	1	18	0	1	32
CXCR4 Chemokine	Human	3ODU [19]	3	0	10	0	0	13
S1PR1 Sphingolipid	Human	3V2Y [20]	9	1	12	0	0	22
NTSR1 Neurotensin	Human	4GRV [21]	17	1	12	0	2	32
PAR1 Protease-activated	Human	3VW7 [22]	9	0	16	0	0	25
		Total	216	22	210	3	22	473

^aInteractions were considered for all pairs of residues having at least two side chain atoms closer than 6.0 Å. Such a large distance cut-off value is justified by the long-range nature of interactions involving sulfur and aromatic groups.

Table 3. List of all interactions involving sulfur-containing amino acids in the crystal structures of 7TMRs

	Res. ^a	Res. ^a	Pair	PDB id ^b
TM1	1.34	1.30	M/W	1GZM
		7.40	C/F	3VW7
	1.35	1.31	M/W	2RH1 2VT4
		1.39	M/M	2RH1 2VT4
	1.39	1.35	M/M	2RH1 2VT4
		1.38	M/Y	1GZM
		2.57	M/Y	4DJH
		2.58	M/F	1GZM
			M/Y	3PBL 4GRV
		7.40	M/F	1GZM
	1.42	1.38	M/W	2RH1 2VT4
			C/Y	3VW7
			C/F	2Z73
	1.43	2.57	C/Y	3V2Y
			M/F	4DJH
	1.44	1.40	M/F	4GRV
			M/F	3RZE
			M/F	1GZM
	1.47	1.44	M/F	1GZM
			C/F	2Z73
	1.54	2.44	M/F	3UON 4DJH 4EA3 4EJ4
	1.57	2.43	M/F	3VW7
			M/Y	3ODU
TM2	2.38	2.42	M/Y	3ODU
		2.40	M/Y	3V2Y
	2.41	4.39	M/H	2Z73
			C/Y	3PBL
			M/F	2Z73
	2.43	1.57	M/F	3VW7
			M/Y	3VW7
	2.48	2.44	C/F	3UON
			M/F	2Z73
			C/W	3UON
	2.53	2.58	M/F	1GZM
			M/F	1GZM
			M/W	1GZM 2RH1
			M/Y	2RH1
	2.57	1.39	C/F	3ODU 3VW7
			1.43	M/Y
C/Y				3V2Y
M/F			4DJH	
M/Y			3V2Y	
M/Y	4DJH			
2.58	1.39	M/F	1GZM	
		M/F	1GZM	
		M/Y	3PBL 4GRV	
		M/F	4GRV	
		M/W	3RZE 3UON 4DAJ	
		M/Y	3PBL 3RZE 3UON 4DAJ 4GRV	
2.60	3.24	C/W	3PBL	
		M/W	3RZE	
2.62	3.28	M/Y	2Z73	
		M/M	2Z73	
2.66	1.32	C/Y	2Z73	
		C/Y	2Z73	
TM3	3.22	3.23	C/H	4EIY
		3.25	C/C	4EIY
			C/F	2Z73
	3.24	2.60	C/W	3PBL

Table 3 (Continued)

	Res. ^a	Res. ^a	Pair	PDB id ^b
TM4	3.25	2.64	C/Y	3RZE
		3.22	C/C	4EIY
			C/F	2Z73
		3.28	C/W	2RH1 2VT4
	3.29	C/F	3PBL	
			C/H	3ODU
		C/Y	4GRV	
	5.30	C/C	2RH1 2VT4	
			C/Y	4EIY
	3.30	5.37	C/Y	4EIY
			M/F	1GZM
	3.31	2.53	M/F	3RZE
			M/F	3RZE
			M/Y	3V2Y
	3.32	2.57	M/F	3VW7
			M/M	3PBL
	3.34	4.50	M/W	3PBL
			C/W	3VW7
			M/F	3PBL
			M/Y	4EJ4
	3.35	3.34	M/M	3PBL
			M/F	2Z73
			C/W	2RH1 2VT4 4GRV
			M/W	3PBL
	3.36	3.32	M/F	3VW7
			M/Y	3VW7 4DJH 4EJ4
			M/Y	3VW7
			M/F	4DJH 4EA3 4EJ4
			M/F	4EA3
			C/F	3PBL
			C/W	3PBL
			M/F	3VW7
	6.52	C/W	4DJH 4EA3 4EJ4	
			M/H	4DJH 4EJ4
			M/F	2Z73
			M/F	2Z73
	3.38	2.48	M/F	2Z73
			M/F	2Z73
			M/W	2Z73
	3.41	3.44	C/W	3PBL
			M/M	2Z73
			M/F	2Z73
			C/F	3V2Y 4EIY
			M/W	2Z73
	3.43	6.44	M/W	1GZM
			M/W	1GZM
	3.44	6.48	M/F	2Z73 3VW7
M/F			3VW7	
3.45	3.41	C/W	3PBL	
		M/F	3RZE	
		M/F	2Z73	
3.46	2.42	M/Y	4DJH 4EJ4	
		M/Y	4EJ4	
		M/M	2Z73	
		M/M	2Z73	
3.47	5.57	M/F	2Z73	
		M/F	2Z73	
3.54	3.51	M/Y	3V2Y	
		C/Y	1GZM 4EA3 4EJ4 4GRV	
		C/Y	1GZM 4EA3 4EJ4 4GRV	
4.37	2.42	M/F	2Z73 2VT4	
		M/M	2Z73	
4.39	2.41	M/H	2Z73	
		C/Y	3PBL	

Table 3 (Continued)

	Res. ^a	Res. ^a	Pair	PDB id ^b	
TM5	4.43	2.41	M/F	2Z73	
		4.44	M/M	3UON	
			M/H	1GZM	
	4.45	M/M	3UON		
	4.45	2.42	M/F	2Z73	
		3.45	M/M	2Z73	
		4.37	M/M	2Z73	
	4.44	4.41	M/M	3UON	
			M/H	1GZM	
		4.45	M/M	3UON	
	4.45	2.42	M/F	3UON 4DAJ	
		4.41	M/M	3UON	
		4.44	M/M	3UON	
	4.46	2.42	C/Y	3VW7	
		2.45	C/H	3VW7	
		4.50	C/W	3VW7	
	4.48	3.41	M/F	2Z73	
		3.45	M/F	2Z73	
	4.49	3.41	C/F	3V2Y 4E1Y	
		4.50	C/W	3V2Y	
	4.52	3.41	M/W	1GZM	
		4.48	M/F	1GZM	
		5.46	M/H	1GZM	
	4.56	5.38	C/F	1GZM	
		5.41	C/Y	1GZM	
		5.46	C/H	1GZM	
	4.58	4.54	C/F	3PBL	
		4.62	C/F	3PBL	
	4.60	3.29	M/F	2VT4	
			M/Y	4GRV	
	4.61	3.23	M/H	4E1Y	
		3.27	M/F	4E1Y	
		3.34	M/Y	4EJ4	
	4.62	3.23	M/F	2VT4	
		4.58	C/F	3PBL	
			M/F	2VT4	
	4.63	5.38	M/F	4EA3	
	4.64	5.41	C/W	2Z73	
	5.30	2.64	C/H	2RH1	
			C/W	2RH1 2VT4	
		5.35	5.38	M/M	4E1Y
			6.59	M/F	4E1Y
			7.29	M/H	4E1Y
		5.38	3.33	M/Y	4DJH
			4.56	C/F	1GZM
			4.63	M/F	4EA3
			5.35	M/M	4E1Y
5.37			M/F	4DJH	
5.41			M/Y	4E1Y	
			5.41	M/F	3RZE
			C/F	4EA3	
5.42			M/F	1GZM	
6.52		M/H	4E1Y		
5.41	4.56	C/W	2Z73		
	4.56	C/Y	1GZM		
	4.64	C/W	2Z73		
	5.37	M/W	3RZE		
	5.38	C/F	4DJH		
		M/F	3RZE		
	C/F	4EA3			
	5.42	M/Y	1GZM		
	5.45	C/F	4DJH 4EA3 4EJ4		
5.46	C/F	4E1Y			

Table 3 (Continued)

	Res. ^a	Res. ^a	Pair	PDB id ^b
TM6	5.42	3.37	M/F	2Z73
		5.38	M/F	1GZM
		5.41	M/Y	1GZM
		5.43	M/F	1GZM
			C/F	3V2Y
		5.46	M/H	1GZM
	5.43	3.33	C/F	3V2Y
		5.39	C/Y	3V2Y
		5.42	C/F	3V2Y
		5.42	M/F	1GZM
		5.47	C/F	3V2Y
		6.56	C/F	4E1Y
	5.44	5.40	M/F	3ODU
		5.45	M/F	4GRV
		6.56	C/F	4E1Y
	5.45	3.37	M/Y	4GRV
		5.41	C/F	4DJH 4EA3 4EJ4
		5.44	M/F	4GRV
		5.49	M/F	4GRV
	5.46	4.52	M/H	1GZM
		4.56	C/H	1GZM
		5.41	C/F	4E1Y
		5.42	M/H	1GZM
	5.51	5.47	M/F	4GRV
		6.44	M/F	4GRV
	5.54	3.44	M/F	3RZE
		5.58	M/Y	2RH1 3UON 4E1Y
		6.41	M/M	2RH1 2VT4 3RZE
		6.44	M/F	2RH1 2VT4 3RZE 3UON 4DAJ
	5.57	3.47	C/F	3RZE
		3.51	C/Y	1GZM 2Z73 3ODU 4DJH 4EA3 4EJ4
			C/F	3VW7
		5.56	C/F	1GZM 2Z73
		5.58	C/Y	4DJH
	5.61	3.51	M/Y	4DJH 4EA3 4EJ4
		5.58	M/Y	4DJH 4EA3 4EJ4
	5.63	5.59	M/F	2Z73
	6.27	6.26	M/H	3RZE
		6.40	M/M	1GZM
	6.36	7.53	M/Y	1GZM 3PBL 4EJ4
		7.56	M/M	1GZM
			M/F	3PBL
		6.40	6.36	M/M
	6.41	5.54	M/M	2RH1 2VT4 3RZE
		5.58	M/Y	2RH1 3RZE
		6.42	C/F	3VW7
	6.42	6.41	C/F	3VW7
6.47	6.48	C/W	1GZM 3PBL 3V2Y 4DJH 4EA3 4EJ4 4GRV	
		C/F	3VW7	
	7.41	C/F	1GZM	
	7.44	C/F	3ODU	
	7.48	C/Y	1GZM	
	6.54	6.51	C/F	2RH1
			M/Y	3UON 4DAJ
		7.30	C/F	3RZE
		7.34	M/Y	4DAJ
		7.35	M/W	3UON 4DAJ
7.38		C/F	4DJH 4EA3 4EJ4	
7.39		M/Y	3UON	

Table 3 (Continued)

	Res. ^a	Res. ^a	Pair	PDB id ^b
	6.56	5.43	C/F	4E1Y
		5.44	C/F	4E1Y
		5.48	M/Y	3RZE
		6.60	C/F	4E1Y
	6.57	6.61	C/F	4E1Y
		7.30	M/F	4GRV
		7.31	M/Y	4GRV
		7.34	M/F	4GRV
	6.59	5.35	M/F	4E1Y
		6.58	C/F	4GRV
		6.60	C/Y	4GRV
	6.61	6.57	C/F	4E1Y
6.60		C/F	3UON	
7.29		C/C	3V2Y	
TM7	7.29	5.35	M/H	4E1Y
		6.61	C/C	3V2Y
		7.35	M/H	4E1Y
	7.30	6.54	C/F	3RZE
		6.57	M/F	4GRV
	7.35	6.51	M/Y	1GZM
		6.54	M/W	3UON 4DAJ
		7.29	M/H	4E1Y
		7.36	M/Y	4E1Y 4GRV
	7.36	7.33	M/Y	4GRV
		7.35	M/Y	4E1Y
			M/Y	4GRV
		7.40	M/W	3RZE
	7.38	6.54	C/F	4DJH 4EA3 4EJ4
		7.37	C/F	4DJH
	7.40	1.34	C/F	3VW7
		1.38	M/F	2Z73
		1.39	M/F	1GZM
			M/W	2RH1 2VT4
			C/Y	3VW7
		1.43	C/W	3RZE
2.58		M/W	3RZE 3UON 4DAJ	
2.62		M/M	2Z73	
7.36		M/W	3RZE	
7.42	6.48	C/W	3UON 4DAJ	
	6.51	C/Y	3UON 4DAJ	
	7.39	C/Y	4DAJ	
7.46	2.53	C/F	3ODU 3VW7	
	7.43	C/F	3ODU	
	7.45	C/H	3ODU	
7.47	7.44	C/F	3ODU	
7.51	7.48	M/H	2Z73	
	7.52	7.53	C/Y	3UON
7.56	7.56	C/C	3UON 4DAJ	
		6.36	M/M	1GZM
		M/F	3PBL	
	6.39	C/F	3RZE	
	7.52	C/C	3UON 4DAJ	

^aResidue number according to Ballesteros and Weinstein [23].

^bSee Table 2 for correspondence between PDB id and receptor name.

this series of interactions could serve to modulate ligand binding, being sensitive, for example, to allosteric modulators [43]. In the β_1 AR, M82^{2.53}V mutation in the analogous residue had a thermostabilizing effect and was employed to successfully crystallize the receptor [44]. This could be explained by a different conformation of

Tyr316^{7.43} that would restrain the receptor in an inactive state. Interestingly, crystal structures of histamine H1, dopamine D3, muscarinic M2, muscarinic M3, and κ opioid receptor (κ OR) feature Met^{2.58} (instead of Met^{2.53}) interacting with Tyr^{7.43}. Figure 1B shows that residue Met83^{2.58} in D3R structure can clearly modulate the conformation of Tyr373^{7.43} in the same manner as Met^{2.53} in β_1 AR and β_2 AR.

The crystal structure of squid rhodopsin also contains a large patch of consecutive interactions involving various Met–Met extending across the membrane along TM4 and reaching intracellular loop (ICL) 2 (Figure 1C). In the same structure, a group of three Met residues connects the C-terminal region of the unusually large TM5 and ICL2 featuring a triangle of Met–Met interactions that also involves H230 (Figure 1D).

In the following subsections, we will show that interactions involving these types of residues are often present in the available repertoire of crystal structures of 7TMRs and are involved in critical aspects of receptor pharmacology and functioning such as receptor–ligand interactions or activation microswitches.

Met–aromatic interactions relevant for ligand binding

Various examples of Met–aromatic interactions are involved in ligand recognition. Figure 2A displays the binding of JDTC to κ OR as a representative model for OR/ligand complexes. It can be seen that in addition to Asp138^{3.32} (the main anchoring point for opioid ligands), Met142^{3.36} forms a Met–aromatic interaction with the ligand that might significantly contribute to binding energy and might equally be important in setting ligand orientation. Interestingly, Met^{3.36} is fully conserved in OR of all species and the four structures for this subfamily of receptors available exhibit similar Met–aromatic interactions with their respective ligands [12–15]. In fact, it is known from structure/activity relationship studies that the aromatic moiety of peptidic or nonpeptidic opioid ligands involved in this interaction is crucial for recognition by cognate receptors [45,46]. Sequence analysis of human class A 7TMRs (performed with the program GMoS, available at <http://lmc.uab.cat/gmos>) shows that Met^{3.36} is present in 31 additional 7TMRs for peptides and 9 7TMRs for nucleotides. In the human melanocyte-stimulating hormone receptor, Met128^{3.36}L substitution significantly decreased agonist potency for an endogenous peptide analog [47]. This suggests that the recognition of ligand aromatic residues by Met^{3.36} could also be relevant in additional receptors.

The large repertoire of A_{2A} adenosine receptor structures also offers beautiful examples of Met–aromatic interactions within the orthosteric-binding sites [17,18]. Specifically, Met117^{5.38} and Met270^{7.35} interact with all crystallized A_{2A}R ligands. Figure 2B displays the binding mode for agonist ZM241385 to A_{2A}R as a representative case. Interestingly, M270^{7.35}I mutation in dog A₁R (the only A₁R containing Met at this position) changed binding affinities of specific agonist and antagonists ligands [48]. The sequence analysis shows that Met^{5.38} is conserved in 85% adenosine receptors and 12% purinoceptors, whereas Met^{7.35} is mostly found in

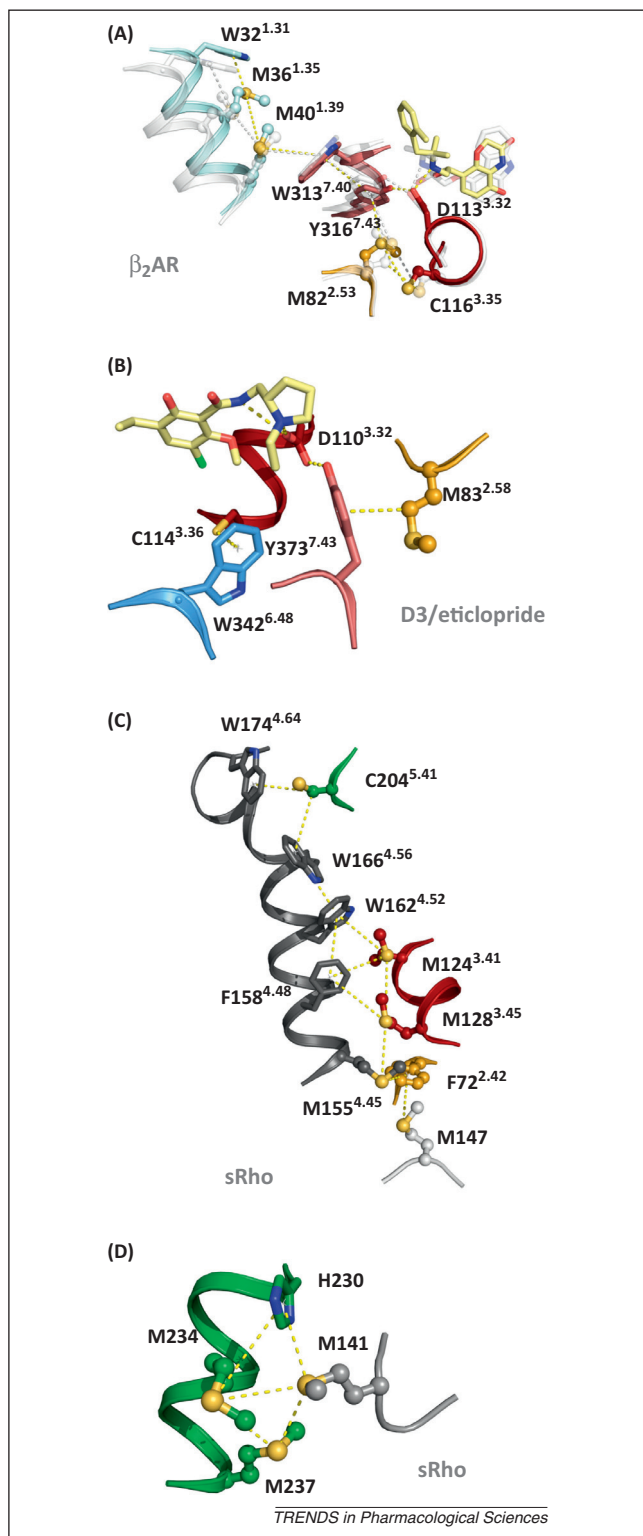


Figure 1. Examples of large Met/Cys–aromatic and Met/Cys–Met interaction patches taken from crystal structures of seven-transmembrane receptors (7TMRs). **(A)** A patch of interactions connect Asp113^{3.32} (the most important ligand-binding element) and the extracellular parts of transmembrane 1 (TM1) and TM7 in β_2 adrenergic receptor (β_2 AR) bound to inverse agonist carazolol (light-gray; PDB id: 2RH1 [5]) and to agonist BI167107 (colored; PDB id: 3SN6 [6]). **(B)** The crystal structure of dopamine D3 receptor (D3R) in complex with eticlopride reveals the presence of two sulfur–aromatic interactions in the vicinity of the ligand-binding pocket: Cys114^{3.36}–Trp342^{6.48} and Met82^{2.58}–Y316^{7.43} (PDB id: 3PBL [9]). **(C)** A patch of interactions in squid rhodopsin propagates along TM4 involving residues from TM2, TM3, and TM5 and from intracellular loop (ICL) 2 (PDB id: 2Z73 [4]). **(D)** A cluster of three Met–Met interactions (also involving H230) in the intracellular part of TM5 and ICL2 in squid rhodopsin (PDB id: 2Z73 [4]). Pieces of TM helices and loops are shown as a cartoon, relevant residues are shown as

A_2 -type receptors (92% conserved), in 13% peptide receptors, and 44% rhodopsins. In angiotensin II type 1 receptor, mutations of residue Met284^{7.35} to Ala or Cys resulted in significantly impaired binding of antagonists [49,50].

The structure of the sphingosine 1-phosphate receptor 1 (S1PR1) in complex with a sphingolipid mimic [20] provides an additional example of Met–aromatic interaction between receptor and ligand (Figure 2C). Here the ligand central phenyl ring interacts with Met124^{3.32}. The sequence analysis shows that this amino acid is also present in most prostanoid receptors, S1PR3, melatonin MT₁, and cholecystokinin receptors 1 and 2 (CCK1R and CCK2R). In CCK1R and CCK2R, Met^{3.32} is a critical residue for binding and activation (see below).

Met–Met and Met–aromatic interactions in 7TMR activation

In β_2 ARs, comparison between carazolol and BI167107 bound structures (representing inactive and active-like states, respectively) reveals a rearrangement of TM5–TM6 interface that involves two Met residues (Met215^{5.54} and Met279^{6.41}) that accompany TM6 opening during activation [5,6]. These residues are part of a network of aromatic–aromatic and Met–aromatic interactions connecting residues Tyr219^{5.58} and Phe282^{6.44}. This ultimately serves to link functionally relevant Trp286^{6.48} and Tyr219^{5.58}, producing a conformational change in Tyr219^{5.58} (Figure 3A). The importance of interactions involving Met215^{5.54} and Met279^{6.41} is supported by their simultaneous presence in more than one-third of the amine receptor sequences and in more than half of the chemokine receptors.

Met^{5.54} and Phe^{6.44} residues are fully conserved in adenosine receptors of all species. Thus, A_{2A} crystal structures follow a similar pattern to β_2 AR structures: lack and formation of interaction between Met193^{5.54} and Phe242^{6.44} in the inactive and in the active structure, respectively [16,17]. Sequence analysis shows that Met^{5.54} and Phe^{6.44} are present in 29% and 80%, respectively, of human receptors and, more important, that 25% of receptors have the Met^{5.54}–Phe^{6.44} pair.

Despite that the Met^{5.54}–Phe^{6.44} pair is not present in rhodopsins, a comparison between dark-state bovine rhodopsin and metarhodopsin II structures also reveals changes in Met–aromatic and Met–Met interactions between TM5 and TM6 (Figure 3B) [2,3]. In the dark-state structure, Met253^{6.36} interacts with Tyr301^{7.53} (of the NPxxY motif), whereas Met257^{6.40} (located one turn after Met253^{6.36}) does not participate in any Met–aromatic interaction. In metarhodopsin II, Tyr301^{7.53} has lost the interaction with Met253^{6.36} and becomes the partner of Met257^{6.40}. In turn, Met257^{6.40} also interacts with Tyr223^{5.58} and forms a Met–Met interaction with Met253^{6.36}. The importance of Met257^{6.40} is manifested

sticks, and sulfur-containing residues as balls and sticks. The color code for helices and loops is: TM1, cyan; TM2, gold; TM3, red; TM5, green; TM6, blue; TM7, pale-red; loops, gray. Ligands are shown in pale-yellow with noncarbon atoms colored by atom type. See Table 4 for characterization of Met/Cys–Met and Met/Cys–aromatic interactions displayed here.

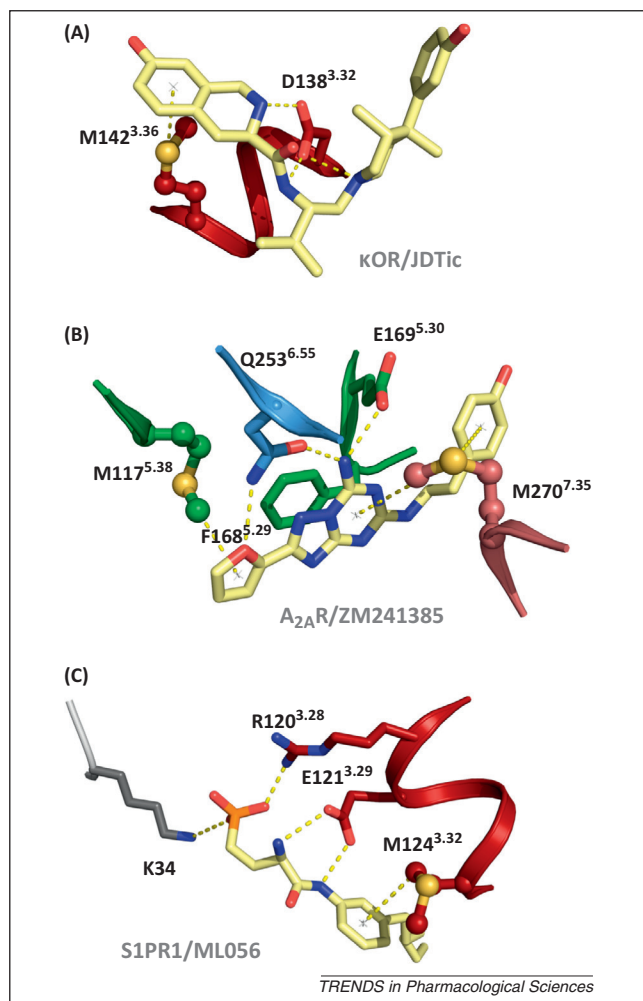


Figure 2. Met–aromatic interactions between ligand and receptor in crystal structures of seven-transmembrane receptors (7TMRs). **(A)** The four opioid receptors (κ OR/JDTic structure is displayed as representative) exhibit an interaction between Met142^{3.36} and an aromatic group in the ligand (PDB id: 4DKL [12]). **(B)** Two Met–aromatic interactions involving Met117^{5.38} and Met270^{7.35} are present in the A_{2A}R/ZMA241385 complex (PDB id: 4E1Y [16]). **(C)** The crystal structure of sphingosine 1-phosphate receptor 1 (S1PR1) in complex with a sphingolipid mimic reveals the presence of an interaction between Met124^{3.32} and an aromatic group in the ligand (PDB id: 3V2Y [20]). Protein representations and colors are the same as in Figure 1. Residues participating in relevant hydrogen bonds with the ligand are also displayed. See Table 4 for characterization of Met/Cys–Met and Met/Cys–aromatic interactions displayed here.

by the observation that M257^{6.40}Y mutation is a constitutively active receptor [51]. The recent crystal structure of this mutant receptor shows that the two residues (Met and Tyr) are able to interact with Tyr223^{5.58} and Tyr301^{7.53} in a similar manner, with only minor changes to the overall structure [52]. This triad of residues has been proposed to be responsible for breaking the Arg135^{3.50}–Glu247^{6.30} ionic lock and for opening up the G protein-binding site [27]. The most notable difference is the formation of a hydrogen bond between Tyr257^{6.40} and Arg135^{3.50} that would be responsible for displacing the equilibrium from inactive to active states. Interestingly, sequence analysis shows that Met^{6.36} and Met^{6.40} are simultaneously present in 85% of vertebrate rhodopsins, a fact that reinforces the functional role of the two amino acids. In addition, Met^{6.36} alone is present in 20% of human 7TMRs, mostly peptide receptors.

Also in rhodopsin, Met207^{5.42} and Met288^{7.35} interact with various aromatic residues surrounding the β -ionone

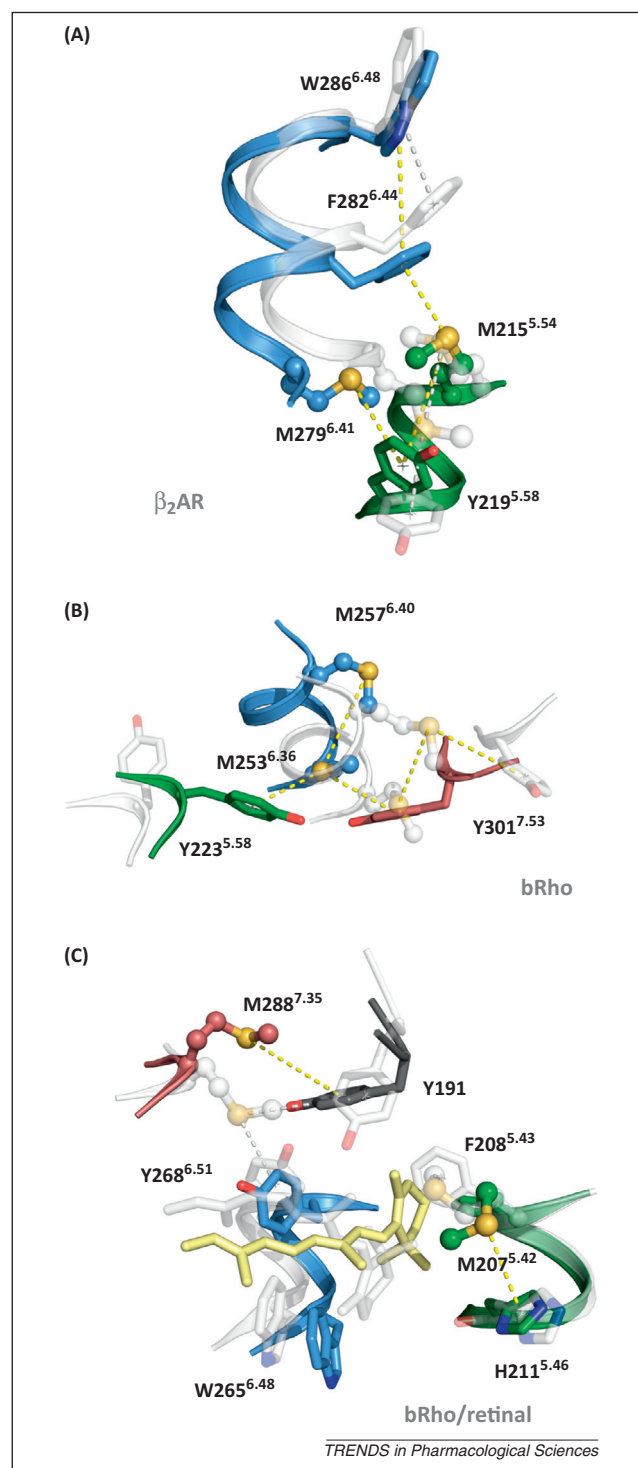


Figure 3. Met–aromatic and Met–Met interactions changing from inactive to active-like crystal structures. **(A)** Changes in the conformations of Met215^{5.54} and Met279^{6.41} in β_2 adrenergic receptor (β_2 AR) crystal structures that could modulate the transmembrane (TM)5/TM6 interface (PDB id: 2RH1 [5] and 3SN6 [6]). **(B, C)** Changes on Met–Met and Met–aromatic interactions (Met257^{6.40} and Met253^{6.36}) in rhodopsin structures in the cytoplasmic side of TMs 5–7 (B) and around the binding site of retinal (PDB id: 1GZM [2] and 3PQR [3]). Protein representations and colors are the same as in Figure 1. The inactive structures are shown in light-gray. See Table 4 for characterization of Met/Cys–Met and Met/Cys–aromatic interactions displayed here.

ring of retinal (Figure 3C). The fact that Met^{7.35} is common to A_{2A}R and that the side chain of Met207^{5.42} is able to reach the same location as Met^{5.38} in A_{2A}R suggests an analogous role for these residues in the two receptors

(Figure 2B). In the inactive bovine rhodopsin structure, Met207^{5,42} interacts with Phe208^{5,43} and Tyr191 in extracellular loop (ECL) 2, whereas Met288^{7,35} is surrounded by Tyr268^{6,51}, Tyr190, and Tyr191. In metarhodopsin II, Met207^{5,42} establishes a new interaction with His211^{5,46} to the detriment of previous interactions with aromatic residues. In parallel, Met288^{7,35} loses the interactions with Tyr268^{6,51}. These changes are consistent with NMR signals associated with Met288^{7,35} and with the suggestion that translation of Phe208^{5,43} after the β -ionone ring relocation of retinal favors the conformational change at the cytoplasmic side of TM5 that ends in Tyr223^{5,58} [27,28]. Sequence analysis shows that 53% of vertebrate rhodopsins have both Met^{5,42} and Met^{7,35}. As an indication of the specific functional role of Met^{5,42}, rhodopsins containing M^{5,42}L mutation give pigments with blue-shifted λ_{\max} [53].

Met/Cys–aromatic interactions in 7TMRs suggested by biophysical studies

At least two groups have recently employed biophysical techniques to elegantly address the importance of interactions involving Met and Cys. First, fluorination experiments were performed on the indole ring of Trp386^{6,48} in the dopamine D2 receptor (D2R), with the aim of characterizing the role of this residue in receptor activation [54]. Progressive fluorination of Trp386^{6,48} diminished the negative electrostatic potential at the aromatic ring surface. The observed trend regarding activation was indicative of a functionally important interaction at the face of the aromatic ring. In particular, tetrafluorination of Trp386^{6,48} resulted in a 300-fold shift in activation potency. Using the crystal structure of D3R in their search for potential partners of Trp^{6,48}, the authors identified Cys^{3,36} as the only residue that could be responsible for the interaction impaired by Trp386^{6,48} fluorination. Thus, it was proposed that this Cys–aromatic interaction between Cys118^{3,36} and Trp338^{6,48} constituted a microdomain regulating D2R activation (see Figure 1B, corresponding to Cys114^{3,36} and Trp342^{6,48} in D3R).

As a second example, ¹H–¹³C NMR resonances were utilized in two independent reports to monitor signals from Met residues in β_2 AR [55,56]. In these two studies, the authors found that receptors occupied by pharmacologically distinct ligands featured changes in chemical shifts and intensities in an efficacy-dependent manner for the resonances corresponding to Met82^{2,53}, Met215^{5,54}, and Met279^{6,41}. Furthermore, their signals correlated with the changes on TM helices 5–7 from inactive to active crystal structures (Figure 1), supporting the view that these residues participate in receptor activation. For Met82^{2,53} (whose involvement in a large network of interactions has been discussed above, Figure 1A), comparison between inactive and active crystal structures shows a conformational change where the interaction between Met82^{2,53} and Tyr316^{7,43} is preferentially enabled in the carazolol-bound structures, whereas Met82^{2,53}–Cys116^{3,35} interaction is enhanced in BI167107-bound structure (Figure 2A). Interestingly, changes on Met215^{5,54} and Met279^{6,41} resonances are also compatible with structural changes in carazolol and BI167107 crystal structures discussed in the previous section.

Met–aromatic interactions suggested by site-directed mutagenesis and molecular modeling

Several examples of Met–aromatic interactions in cholecystokinin receptors (CCK1R and CCK2R) that have remarkable pharmacological and functional importance were suggested on the basis of research by our group [23,57–59]. Cholecystokinin peptide (CCK) exhibits a post-translational sulfation of a Tyr residue. This sulfate moiety is essential for biological activity of CCK at CCK1R, contributing very strongly (500–1000-fold) to CCK binding to CCK1R high affinity state. For receptors that have not yet been crystallized, it is still possible to derive insights from models based on X-ray crystal structures. It is reasonable to expect that these models will be accurate in the TM domains considering the current status of 7TMR molecular modeling [60]. Site-directed mutagenesis studies conducted in synergy with molecular modeling suggested that Tyr–SO₃[−] of CCK probably interacts with Arg197 (ECL2) of CCK1R. In addition, the Tyr side chain of this Tyr–SO₃[−] of CCK was found to interact with Met195 in ECL2 (Figure 4A) [57]. Analysis of Met195-mutated CCK1R indicated that the exchange of Met for Leu caused a minor decrease (3-fold) on the affinity of the high affinity sites for CCK, but a strong drop (75%) on the number of sites, despite the number of low affinity-binding sites remaining unchanged. Thus, Met195 is not important for binding affinity of CCK but rather dramatically influenced the amount of CCK1R which could be converted to a high affinity state for CCK. A plausible interpretation for these data was that this Met–aromatic interaction between Met195 and Tyr–SO₃[−] defined a specific positioning of the sulfate group relative to Arg197, stabilizing ligand-bound CCK1R in a high affinity state. Again in CCK1R, Met131^{3,23} was suggested to interact with the C-terminal aromatic group of agonist peptides as it appeared to be essential for Gq-dependent production of the second messengers, inositol phosphates (Figure 4A) [58].

Recently, we have shown in CCK2R that the interaction between Met134^{3,32} and Tyr380^{7,43} governs the equilibrium between two CCK2R states: either coupling to G_q or recruiting β -arrestin 2 (Figure 4B) [59]. This conclusion was reached by mutating Met134^{3,32} and Tyr380^{7,43}, which dramatically affected CCK2R efficacy to recruit β -arrestin 2, whereas the mutations did not affect CCK2R efficacy to activate phospholipase C. The existence of distinct CCK2R conformations associated with G protein-dependent or β -arrestin 2-dependent signaling pathways was further pharmacologically demonstrated using a biased competitive antagonist which inhibited G protein-dependent signaling but not β -arrestin 2-dependent pathways.

As a third example, the thyroid-stimulating hormone receptor (TSHR) exhibits elevated cAMP signaling in the basal state and becomes fully activated by thyrotropin. Two independent studies reported Met mutations generating constitutive active receptors [61,62]. First, M626^{6,37}I produced basal cAMP levels 13-fold higher than wild type TSHR [61]. TSHR structural models suggest that Met626^{6,37} in TSHR probably participates in Met–aromatic interactions that switch from the inactive to the active state (Figure 4C). More precisely, Met626^{6,37} would interact with one face of Tyr601^{5,58} in the inactive state, whereas upon

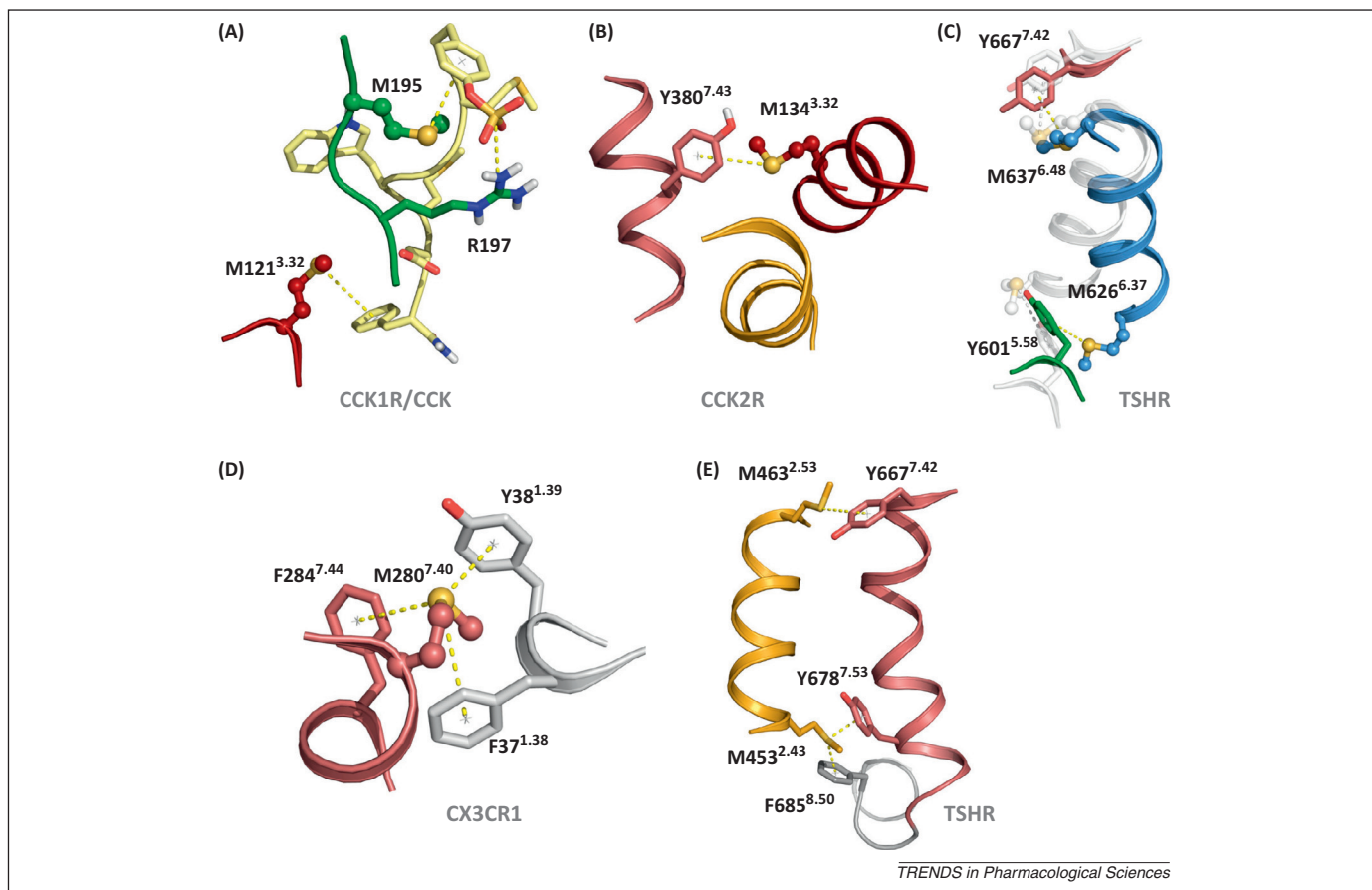


Figure 4. Molecular models for Met–aromatic interactions evidenced from site-directed mutagenesis (A–C) or related to polymorphisms (D–E). Effects of mutations in receptors without available structure are better understood on homology models. (A) Cholecystokinin (CCK) binding to cholecystokinin receptor 1 (CCK1R) involves two Met–aromatic interactions between Phe/Tyr residues of CCK and two Met residues Met195 [in extracellular loop (ECL) 2] and Met121^{3.32}. An ionic interaction is formed between Arg197 and the sulfate group of the Tyr residue of CCK, whose aromatic side chain participates in the aromatic–sulfur interaction with Met195 (model CCK1R_1, adapted from [57,58]). (B) The interaction of Met134^{3.32} and Tyr380^{7.43} in cholecystokinin receptor 2 (CCK2R) is required for receptor signaling through β -arrestin 2 recruitment but not through G protein coupling (model CCK2R_1, adapted from [59]). (C) Comparison between inactive (light-gray transparency) and active-like (colored) thyroid-stimulating hormone receptor (TSHR) models (TSHR_1 and TSHR_2). M6.48W and M6.37I are two constitutively active mutations whose behavior could be due to sulfur–aromatic interactions. (D) The specific phenotype of T280^{7.40}M mutant in CX3CR1 chemokine receptor could be due to Met–aromatic interactions (model CX3CR1_1). (E) In TSHR, Met453^{2.43}T and Met463^{2.53}V polymorphisms cause nonautoimmune hyperthyroidism (model TSHR_1). The two residues would participate in Met–aromatic interactions. Protein representations and colors are the same as in Figure 1. All models were created using Modeller 9.11 and are freely available to readers upon request to the authors [68]. Inactive models for CCK1R (model CCK1R_1), CCK2R (CCK2R_1), and TSHR (TSHR_1) were based on PDB id 4DKL, whereas CX3CR1_1 relied on PDB id 3ODU [19]. The active TSHR model (TSHR_2) was built on PDB id 3SN6 [6]. See Table 4 for characterization of Met/Cys–Met and Met/Cys–aromatic interactions displayed here.

activation (and the outward movement of TM6), it would interact with the opposite face of Tyr601^{5.58}. Thus, M626^{6.37}I mutant would hinder these interactions. The second constitutively active mutant was M637^{6.48}W [62]. All glycoprotein hormone receptors contain Met^{6.48} instead of the conserved Trp present in 80% of 7TMRs. This mutant also displayed atypical pharmacology in that thyrotropin activated it with the same potency as the wild type, whereas the small non-peptide NCGC00161870-01 agonist activated this mutant with a 14-fold decreased potency. The authors proposed that M637^{6.48}W was important for stabilizing the active state by means of Met–aromatic interactions between residue Tyr667^{7.42} and an aromatic moiety in the ligand. Sequence analysis indicates that the Met637^{6.48}/Tyr667^{7.42} pair is conserved in glycoprotein hormone receptors, suggesting that this interaction could have functional importance.

Polymorphisms associated with introduction/disappearance of Met residues

Various polymorphisms in 7TMRs that affect or introduce Met residues have been described. Because of the specific

interactions between Met and aromatic residues, these polymorphisms are likely to modify receptor dynamics and thus raise significant changes in phenotype. T280^{7.40}M mutation in the CX3CR1 chemokine receptor constitutes a first example. Patients having this mutation who were infected with HIV-1 virus showed a rapid progression to AIDS [63]. A homology model of CX3CR1 (Figure 4D) suggests that Met280^{7.40} would exhibit two Met–aromatic interactions with Phe37^{1.38} and Tyr38^{1.39} that may stabilize a specific receptor conformation-promoting activation.

In TSHR, M453^{2.43}T and M463^{2.53}V are two activating mutations causing nonautoimmune hyperthyroidism [64,65]. Homology models of the inactive TSHR (Figure 4B) show that Met453^{2.43}, located at the cytoplasmic side of TM2, interacts with conserved Tyr678^{7.53} and Phe685^{8.50}. Thus, it is likely that the M453^{2.43}V mutation affects the equilibrium between inactive and active states, leading to constitutive activity. By contrast, Met463^{2.53}, located at the region of closest contact between TM2, TM3, and TM7 could participate in a Met–aromatic

Table 4. Characterization of Met/Cys–Met and Met/Cys–aromatic interactions displayed in Figures 1–4

		Receptor	Interaction	Type ^a	Inactive		Active				
					d (Å) ^b	θ (°) ^c	d (Å) ^b	θ (°) ^c			
Figure 1	a	β ₂ AR	M1.35–W1.31	CH _{2/3} –π/S–π	5.1	49.7	3.7	45.2			
			M1.35–M1.39	CH _{2/3} –S	5.3	27.2	6.5	55.7			
			M1.39–W7.40	S–π, CH _{2/3} –π	5.4	51.0	5.6	51.2			
			M2.53–Y7.43	CH _{2/3} –π/S–π	5.4	60.0	4.3	47.0			
			M2.53–C3.35	CH _{2/3} –S	4.9	72.8	4.9	37.7			
	b	D3	M2.58–Y7.43	S–CH	4.9	36.2					
			C3.36–W6.48	SH–π	3.8	56.6					
	c	sRhod	C5.41–W4.64	CH–S	4.5	64.7					
			C5.41–W4.56	S–π	5.4	20.5					
			M3.41–F4.48	CH–S	5.2	72.3					
			M3.41–W4.52	CH _{2/3} –π	5.2	27.1					
			M3.41–M3.45	CH _{2/3} –S	5.3	61.3					
			M3.45–F4.48	–	5.7	80.4					
			M3.45–M4.45	CH _{2/3} –S	4.8	80.9					
			M4.45–F2.42	CH–S	5.2	78.4					
			M4.45–M147	CH _{2/3} –S	4.0	55.5					
			M147–F2.42	CH–S	5.3	70.6					
d	sRhod	M234–H230	CH _{2/3} –π	5.9	58.0						
		M234–M141	CH _{2/3} –S	4.9	80.0						
		M234–M237	CH _{2/3} –S	4.9	26.8						
		M141–M237	CH _{2/3} –S	3.9	40.4						
		M141–H230	CH–S	4.2	80.2						
Figure 2	a	κOR	M3.36–JDTic	S–π	5.5	22.4					
	b	A _{2A}	M5.38–ZM (furan)	CH _{2/3} –π	5.1	22.0					
			M7.35–ZM (Tyr)	CH _{2/3} –π	5.8	62.0					
			M7.35–ZM (triazine)	CH _{2/3} –π	6.2	39.1					
c	S1PR	M3.32–ML	CH _{2/3} –π	4.9	16.7						
Figure 3	c	β ₂ AR	M5.54–F6.44	S–π	7.0	51.7	4.0	24.0			
			M5.54–M6.41	CH _{2/3} –S	4.4	25.8	5.0	58.6			
			M6.41–Y5.58	S–π	3.9	14.3	4.9	68.2			
			M5.54–Y5.58	CH _{2/3} –π	7.9	35.5	6.2	37.0			
	g	bRhod	M6.36–M6.40	CH _{2/3} –S	4.9	47.4	6.0	38.4			
			M6.40–Y7.53	CH–S	5.6	40.6	4.8	57.3			
			M6.40–Y5.58	CH–S	14.6	–	4.2	42.9			
	f	bRhod	M5.42–H5.46	S–π	7.7	63.8	4.3	32.4			
			M5.42–F5.43	CH–S/S–π	5.6	19.6	10.4	71.9			
			M7.35–Y6.51	S–π, CH _{2/3} –π	4.2	49.7	8.9	65.0			
			M7.35–Y191	CH–π	6.8	67.9	6.3	16.6			
			Figure 4 ^d	a	CCK1	M3.32–CCK (Phe)	S–π	4.9	14.3		
						M195–CK (TyrSO4)	CH _{2/3} –π	4.4	66.4		
b	CCK2	M3.32–Y7.43		S–π	4.5	62.5					
c	TSHR	M6.37–Y5.58	CH–S	5.4	88.5	5.0	62.1				
		M6.48–Y7.42	CH–S	5.0	87.5	4.4	79.3				

^aCH_{2/3}–S and CH–S account for CH(alkyl)–S and CH(arene)–S interactions, respectively; ‘/’ indicates changes from the inactive to the active-like structure.

^bSulfur–ring centroid (or sulfur–sulfur) distance.

^cθ Angle between the normal vector to the aromatic plane (or Met/Cys plane) and the sulfur atom defined as in [31,34,36].

^dApproximate values from molecular models (in gray).

interaction with Tyr667^{7,42}. This interaction could play a similar role as the Met134^{3,32}–Tyr380^{7,43} interaction in CCK2R, which was found to govern G protein-dependent signaling but not β-arrestin 2-dependent pathways.

Concluding remarks

7TMRs feature several examples of Met/Cys–aromatic and Met–Met interactions that are, in some cases, responsible for important pharmacological, signaling, or functional events. In the present review, we have described many examples of such interactions occurring between natural or

synthetic ligands and their receptors, and between two or more residues within the receptor (Figures 1–4 and Table 4). In ligand–protein complexes, interactions involving Met and Cys could, for example, provide additional binding energy and also modulate ligand orientation within the binding site. Within the receptor, we have shown that these interactions might help to stabilize specific conformations. In fact, for receptors for which an active crystal structure is available, comparison between inactive and active structures shows changes associated with formation/breakage of interactions involving Met residues. Met

residues can easily change side chain conformation within a packed environment and, thus, offer extra versatility to respond to structural changes compared to aromatic rings [66]. In addition, the intrinsic flexibility of Met might enable optimization towards energetically favorable Met–Met or Met–aromatic arrangements. These interactions are more directional than the interactions between aliphatic chains, a fact that makes them very useful to keep aromatic residues in well-defined orientations. In terms of strength, Met/Cys–aromatic and Met–Met interactions are stronger than other already widely accepted interactions such as those between two aromatic residues.

Analysis of crystal structures for the 17 members of the 7TMR family has identified a large number of such interactions. Because of the relatively low prevalence of positions containing Cys or Met in 7TMRs [67], the interactions described in this report are highly subfamily-specific, suggesting that Met–Met and Met/Cys–aromatic interactions are often employed for fine-tuning receptor function within subfamilies. The Met^{5.54}–Phe^{6.44} interaction is a remarkable exception, being present in up to 25% of human class A 7TMRs. Thus, this constitutes the most representative example of a Met/Cys–aromatic interaction associated with residues with known functional implication in 7TMRs. Also, involvement of such interactions in ligand binding to 7TMRs suggests that exploiting this relatively unused Met–aromatic interaction may be an original way to design new ligands that may have therapeutic interest. Finally, the recent discovery of a Met–aromatic interaction in CCK2R that was crucial for selective stabilization of protein state associated with β -arrestin 2 recruitment could anticipate that interactions of moderate strength such as Met/Cys–aromatic and Met–Met may play a role in selectively targeting specific signaling pathways, such as those preferentially triggering G protein-dependent or β -arrestin 2-dependent signaling pathways.

Acknowledgments

A.C. is a receiver of a contract grant from ISCIII (Instituto de Salud Carlos III). J.C.G. is a receiver of an FPI (Formación de Personal Investigador) grant from Ministerio de Economía y Competitividad.

References

- Overington, J.P. *et al.* (2006) How many drug targets are there? *Nat. Rev. Drug Discov.* 5, 993–996
- Li, J. *et al.* (2004) Structure of bovine rhodopsin in a trigonal crystal form. *J. Mol. Biol.* 343, 1409–1438
- Choe, H.W. *et al.* (2011) Crystal structure of metarhodopsin II. *Nature* 471, 651–655
- Murakami, M. and Kouyama, T. (2008) Crystal structure of squid rhodopsin. *Nature* 453, 363–367
- Cherezov, V. *et al.* (2007) High-resolution crystal structure of an engineered human β 2-adrenergic G protein coupled receptor. *Science* 318, 1258–1265
- Rasmussen, S.G. *et al.* (2011) Crystal structure of the β 2 adrenergic receptor-Gs protein complex. *Nature* 477, 549–555
- Warne, T. *et al.* (2008) Structure of a β 1-adrenergic G-protein-coupled receptor. *Nature* 454, 486–491
- Shimamura, T. *et al.* (2011) Structure of the human histamine H1 receptor complex with doxepin. *Nature* 475, 65–70
- Chien, E.Y. *et al.* (2011) Structure of the human dopamine D3 receptor in complex with a D2/D3 selective antagonist. *Science* 330, 1091–1095
- Haga, K. *et al.* (2012) Structure of the human M2 muscarinic acetylcholine receptor bound to an antagonist. *Nature* 482, 547–551
- Kruse, A.C. *et al.* (2012) Structure and dynamics of the M3 muscarinic acetylcholine receptor. *Nature* 482, 552–556
- Wu, H. *et al.* (2012) Structure of the human κ -opioid receptor in complex with JDTic. *Nature* 485, 327–332
- Manglik, A. *et al.* (2012) Crystal structure of the μ -opioid receptor bound to a morphinan antagonist. *Nature* 485, 321–326
- Granier, S. *et al.* (2012) Structure of the δ -opioid receptor bound to naltrindole. *Nature* 485, 400–404
- Thompson, A.A. *et al.* (2012) Structure of the nociceptin/orphanin FQ receptor in complex with a peptide mimetic. *Nature* 485, 395–399
- Liu, W. *et al.* (2012) Structural basis for allosteric regulation of GPCRs by sodium ions. *Science* 337, 232–236
- Lebon, G. *et al.* (2011) Agonist-bound adenosine A2A receptor structures reveal common features of GPCR activation. *Nature* 474, 521–525
- Xu, F. *et al.* (2011) Structure of an agonist-bound human A2A adenosine receptor. *Science* 332, 322–327
- Wu, B. *et al.* (2010) Structures of the CXCR4 chemokine GPCR with small-molecule and cyclic peptide antagonists. *Science* 330, 1066–1071
- Hanson, M.A. *et al.* (2012) Crystal structure of a lipid G protein-coupled receptor. *Science* 335, 851–855
- White, J.F. *et al.* (2012) Structure of the agonist-bound neurotensin receptor. *Nature* 490, 508–513
- Zhang, C. *et al.* (2012) High-resolution crystal structure of human protease-activated receptor 1. *Nature* 492, 387–392
- Ballesteros, J.A. and Weinstein, H. (1995) Integrated methods for modeling G-protein coupled receptors. *Methods Neurosci.* 25, 366–428
- Audet, M. and Bouvier, M. (2012) Restructuring G-protein-coupled receptor activation. *Cell* 151, 14–23
- Schwartz, T.W. *et al.* (2006) Molecular mechanism of 7TM receptor activation – a global toggle switch model. *Annu. Rev. Pharmacol. Toxicol.* 46, 481–519
- Liapakis, G. *et al.* (2012) The G-protein coupled receptor family; actors with many faces. *Curr. Pharm. Des.* 18, 175–185
- Goncalves, J.A. *et al.* (2010) Structure and function of G protein-coupled receptors using NMR spectroscopy. *Prog. Nucl. Magn. Reson. Spectrosc.* 57, 159–180
- Deupi, X. *et al.* (2012) Conserved activation pathways in G-protein-coupled receptors. *Biochem. Soc. Trans.* 40, 383–388
- Tauer, T.P. *et al.* (2005) Estimates of the *ab initio* limit for sulfur- π interactions: the H2S-benzene dimer. *J. Phys. Chem. A* 109, 191–196
- Zauhar, R.J. *et al.* (2000) Evidence for a strong sulfur–aromatic interaction derived from crystallographic data. *Biopolymers* 53, 233–248
- Pal, D. and Chakrabarti, P. (2001) Non-hydrogen bond interactions involving the methionine sulfur atom. *J. Biomol. Struct. Dyn.* 19, 115–128
- Samanta, U. *et al.* (2000) Environment of tryptophan side chains in proteins. *Proteins* 38, 288–300
- Duan, G.L. *et al.* (2001) Characterization of aromatic–thiol π -type hydrogen bonding and phenylalanine–cysteine side chain interactions through *ab initio* calculations and protein database analyses. *Mol. Phys.* 99, 1689–1699
- Ringer, A.L. *et al.* (2007) Models of S/ π interactions in protein structures: comparison of the H2S benzene complex with PDB data. *Protein Sci.* 16, 2216–2223
- Cabaleiro-Lago, E.M. *et al.* (2004) Computational study of the interaction in (CH3)(2)X dimer and trimer (X = O, S). *J. Phys. Chem. A* 108, 4923–4929
- Ringer, A.L. *et al.* (2006) Aliphatic C–H/ π interactions: methane–benzene, methane–phenol, and methane–indole complexes. *J. Phys. Chem. A* 110, 10822–10828
- Morgan, R.S. *et al.* (1978) Chains of alternating sulfur and π -bonded atoms in eight small proteins. *Int. J. Pept. Protein Res.* 11, 209–217
- Pranata, J. (1997) Sulfur aromatic interactions: a computational study of the dimethyl sulfide benzene complex. *Bioorg. Chem.* 25, 213–219
- Viguera, A.R. and Serrano, L. (1995) Side-chain interactions between sulfur-containing amino acids and phenylalanine in α -helices. *Biochemistry* 34, 8771–8779
- Sinnokrot, M.O. and Sherrill, C.D. (2006) High-accuracy quantum mechanical studies of π – π interactions in benzene dimers. *J. Phys. Chem. A* 110, 10656–10668

- 41 Janowski, T. and Pulay, P. (2007) High accuracy benchmark calculations on the benzene dimer potential energy surface. *Chem. Phys. Lett.* 447, 27–32
- 42 Tsuzuki, S. *et al.* (2002) Origin of attraction and directionality of the π interaction: model chemistry calculations of benzene dimer interaction. *J. Am. Chem. Soc.* 124, 104–112
- 43 Bokoch, M.P. *et al.* (2010) Ligand-specific regulation of the extracellular surface of a G-protein-coupled receptor. *Nature* 463, 108–112
- 44 Warne, T. *et al.* (2009) Development and crystallization of a minimal thermostabilized G protein-coupled receptor. *Protein Expr. Purif.* 65, 204–213
- 45 Guerrini, R. *et al.* (2000) Structure–activity relationships of nociceptin and related peptides: comparison with dynorphin A. *Peptides* 21, 923–933
- 46 Eguchi, M. (2004) Recent advances in selective opioid receptor agonists and antagonists. *Med. Res. Rev.* 24, 182–212
- 47 Yang, Y. *et al.* (2009) Novel binding motif of ACTH analogues at the melanocortin receptors. *Biochemistry* 48, 9775–9784
- 48 Tucker, A.L. *et al.* (1994) A1 adenosine receptors. Two amino acids are responsible for species differences in ligand recognition. *J. Biol. Chem.* 269, 27900–27906
- 49 Perlman, S. *et al.* (1997) Dual agonistic and antagonistic property of nonpeptide angiotensin AT1 ligands: susceptibility to receptor mutations. *Mol. Pharmacol.* 51, 301–311
- 50 Boucard, A.A. *et al.* (2003) Constitutive activation of the angiotensin II type 1 receptor alters the spatial proximity of transmembrane 7 to the ligand-binding pocket. *J. Biol. Chem.* 278, 36628–36636
- 51 Han, M. *et al.* (1998) Constitutive activation of opsin by mutation of methionine 257 on transmembrane helix 6. *Biochemistry* 37, 8253–8261
- 52 Deupi, X. *et al.* (2012) Stabilized G protein binding site in the structure of constitutively active metarhodopsin-II. *Proc. Natl. Acad. Sci. U.S.A.* 109, 119–124
- 53 Yokoyama, S. *et al.* (1999) Adaptive evolution of color vision of the Comoran coelacanth (*Latimeria chalumnae*). *Proc. Natl. Acad. Sci. U.S.A.* 96, 6279–6284
- 54 Daeffler, K.N. *et al.* (2012) Functionally important aromatic–aromatic and sulfur– π interactions in the D2 dopamine receptor. *J. Am. Chem. Soc.* 134, 14890–14896
- 55 Kofuku, Y. *et al.* (2012) Efficacy of the β_2 -adrenergic receptor is determined by conformational equilibrium in the transmembrane region. *Nat. Commun.* 3, 1045
- 56 Nygaard, R. *et al.* (2013) The dynamic process of β_2 -adrenergic receptor activation. *Cell* 152, 532–542
- 57 Gigoux, V. *et al.* (1998) Met-195 of the cholecystokinin-A receptor interacts with the sulfated tyrosine of cholecystokinin and is crucial for receptor transition to high affinity state. *J. Biol. Chem.* 273, 14380–14386
- 58 Escrieut, C. *et al.* (2002) The biologically crucial C terminus of cholecystokinin and the non-peptide agonist SR-146,131 share a common binding site in the human CCK1 receptor. Evidence for a crucial role of Met-121 in the activation process. *J. Biol. Chem.* 277, 7546–7555
- 59 Magnan, R. *et al.* (2013) Distinct CCK-2 receptor conformations associated with β -arrestin-2 recruitment or phospholipase-C activation revealed by a biased antagonist. *J. Am. Chem. Soc.* 135, 2560–2573
- 60 Kufareva, I. *et al.* (2011) Status of GPCR modeling and docking as reflected by community-wide GPCR Dock 2010 assessment. *Structure* 19, 1108–1126
- 61 Ringkanaanont, U. *et al.* (2006) Repulsive separation of the cytoplasmic ends of transmembrane helices 3 and 6 is linked to receptor activation in a novel thyrotropin receptor mutant (M626I). *Mol. Endocrinol.* 20, 893–903
- 62 Kleinau, G. *et al.* (2011) From molecular details of the interplay between transmembrane helices of the thyrotropin receptor to general aspects of signal transduction in family A G-protein-coupled receptors (GPCRs). *J. Biol. Chem.* 286, 25859–25871
- 63 Becker, Y. (2007) The spreading of HIV-1 infection in the human organism is caused by fractalkine trafficking of the infected lymphocytes – a review, hypothesis and implications for treatment. *Virus Genes* 34, 93–109
- 64 Ferrara, A.M. *et al.* (2007) A new case of familial nonautoimmune hyperthyroidism caused by the M463V mutation in the TSH receptor with anticipation of the disease across generations: a possible role of iodine supplementation. *Thyroid* 17, 677–680
- 65 Kraemer, S. *et al.* (2009) Activating TSH-receptor mutation (Met453Thr) as a cause of adenomatous non-autoimmune hyperthyroidism in a 3-year-old boy. *J. Pediatr. Endocrinol. Metab.* 22, 269–274
- 66 Gellman, S.H. (1991) On the role of methionine residues in the sequence-independent recognition of nonpolar protein surfaces. *Biochemistry* 30, 6633–6636
- 67 Mirzadegan, T. *et al.* (2003) Sequence analyses of G-protein-coupled receptors: similarities to rhodopsin. *Biochemistry* 42, 2759–2767
- 68 Sali, A. and Blundell, T.L. (1993) Comparative protein modeling by satisfaction of spatial restraints. *J. Mol. Biol.* 234, 779–815